UDC 629.5:532.516

SPECIAL-SHAPED LOW-DRAG LAMINAR HULLS TO INCREASE SPEED AND IMPROVE THE COMMERCIAL EFFICIENCY OF FLOATING VEHICLES

I. G. Nesteruk^{1,2}

¹Institute of Hydromechanics of NAS of Ukraine 8/4, Marii Kapnist Str., 03057, Kyiv, Ukraine E-mail: inesteruk@yahoo.com

²Isaac Newton Institute for Mathematical Sciences University of Cambridge United Kingdom

Received 18.06.2024

Slender bodies of revolution with an attached boundary layer can delay its turbulization and ensure low pressure drag. That is why studying of the unseparated rigid bodies, similar in contours to aquatic animals, allowed concluding that the shape itself can provide low drag inherent in laminar flow. The volumetric friction drag coefficient of elongated axisymmetric unseparated hulls reaches its minimum at the critical Reynolds number, which relates their speed, volume, and length with the kinematic viscosity of the fluid and can be used for optimization in unbounded flows of water or air. The characteristics of proposed hulls moving on the water surface are still unknown. Nevertheless, it was shown that special shapes with very sharp concave noses, similar to the fastest fish rostrums, allow removing of stagnation points and high pressures on the body surface. This effect allows reducing the wave resistance. The potential attached flow of inviscid incompressible fluid around a slender body of revolution moving horizontally at constant speed near the water surface was simulated with the use of sources and sinks located on the axis of symmetry and sources and sinks with opposite intensity located on a corresponding line above the water surface. The absence of the pressure peaks and low values of the vertical component of velocities on the water surface were demonstrated for specially shaped bodies of revolution with sharp concave noses for different elongations and depths of movements. For comparison, the same characteristics were calculated for shapes with convex noses. The total drag, commercial efficiency, and maximal displacement of the laminar hull were estimated. Low values of drag yield rather high speeds of movement with the use of standard engines. After corresponding testing, the proposed shapes can be used to reduce the total drag of ships and rowing racing shells and to increase the speed and commercial efficiency.

KEY WORDS: commercial efficiency, drag reduction, environmental protection, unseparated shapes, wave drag

1. INTRODUCTION

Ships or underwater vehicles, which ensure an attached flow pattern on their hulls, are expected to be the most effective since separation causes intensive vortices in the flow, increasing drag and noise. In the case of slender bodies of revolution, the attached flow pattern ensures low-pressure drag and can delay laminar-turbulent transitions on their surfaces [1]. Therefore, the skin-friction drag and total drag can be reduced on such bodies. That is why the unseparated rigid bodies similar to the shape of aquatic animals have attracted great interest from researchers [1–8]. Testing rigid bodies, similar in shape to that of animals and at Reynolds numbers close to those associated with real animals has demonstrated the absence of boundary-layer separation [2]. Attached flow patterns have been observed on gliding dolphins [3].

On the other hand, most researchers believe that the minimum pressure is always located near the midline of the body and renders separation inevitable downstream from the corresponding cross section [9,10]. Nevertheless, theoretical investigations have shown that a pressure decrease is possible near the tail of some specially shaped bodies of revolution (e.g. [4,5,7,8,11–13]). Examples of such hulls were also manufactured and tested in wind tunnels [4,6,13]. Unfortunately, a negative pressure gradient downstream of the maximum thickness section is not enough to remove the separation. For example, on the specially shaped Goldschmied's body [13], the attached flow pattern was achieved only with the use of the boundary layer suction. However, for shapes tested in [4,6] the separation was removed without any active flow control methods. This fact and theoretical estimates of the critical Reynolds numbers of the laminar-to-turbulent transition [1] allowed the conclusion that in underwater motion, the shape itself can provide low drag inherent in laminar flow [5], and very simply solve the well-known Gray paradox concerning the dolphin swimming [14–18].

The fastest fish, e.g., sailfish, swordfish, black marlin, etc. have a maximum swimming speed of around 30 m/s and a very sharp nose – rostrum [2,19–21]. This specific feature of their shape probably allows these animals to remove stagnation points and high pressures on the body surface and to reduce the wave drag when moving near the water surface. The corresponding bodies of revolution with sharp concave noses showed the absence of the pressure peaks on their shape [7] and much lower vertical velocities on the water surface [8]. Since high pressures on the vessel bow and stern cause the waves on the water surface, these specially shaped bodies of revolution with sharp concave noses open up prospects for their use to reduce the wave drag.

After corresponding tower tank experiments, such shapes could be recommended for hulls of small ships and rowing racing shells. In this paper, we will estimate the drag, maximum velocity, and commercial efficiency of specially shaped unseparated floating hulls and their possible application areas.

2. SIMULATION OF THE FLOW NEAR THE WATER SURFACE

We will consider a steady movement of a slender body of revolution along its axis of symmetry at depth h near the water surface, see Fig. 1. When the Reynolds numbers and the length to the diameter ratio L/D are large enough the potential of the flow can be simulated with the use of the sets of sources and sinks with intensities Q_i , located at points $(\xi_i, 0, 0)$, and sources and sinks of inverse intensities $-Q_i$, located at points $(\xi_i, 2h, 0)$ (see

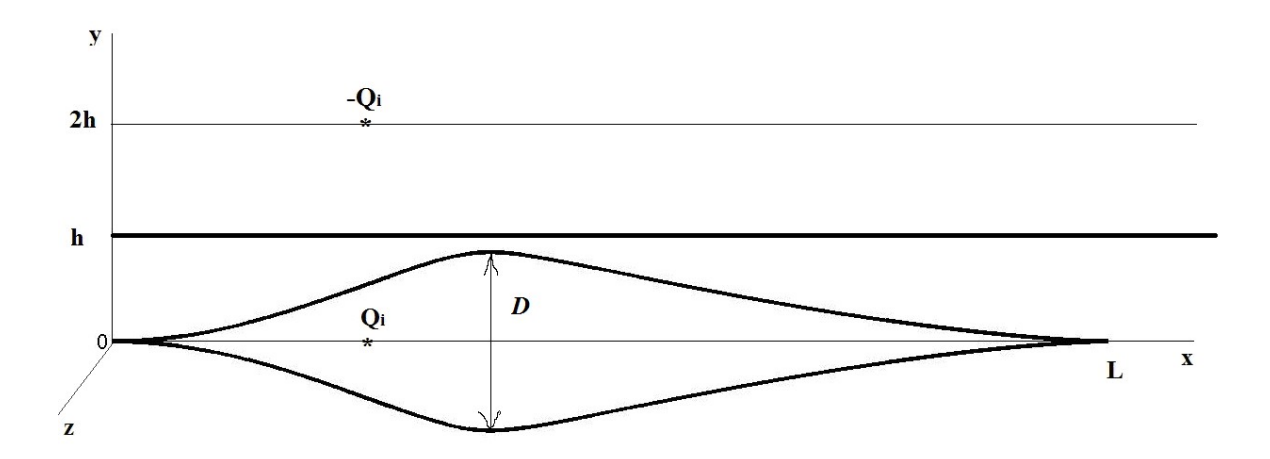


Fig. 1. Body of revolution near the water surface (bold horizontal line) with the length L and maximal diameter D. Simulation of the inviscid incompressible flow using the sources and sinks

Figure 1 in [8]). Differentiation of the potential yields the following formulas for dimensionless components of the velocity (based on the velocity of the body movement U, [8]):

$$v_x = 1 + \sum_{i=1}^{n} v_{ix}, \qquad v_r = \sum_{i=1}^{n} v_{ir},$$
 (1)

$$v_{ix} = \frac{Q_i(x - \xi_i)}{4\pi \left[(x - \xi_i)^2 + y^2 + z^2 \right]^{3/2}} - \frac{Q_i(x - \xi_i)}{4\pi \left[(x - \xi_i)^2 + (y - 2h)^2 + z^2 \right]^{3/2}},$$
 (2)

$$v_{iy} = \frac{Q_i y}{4\pi \left[(x - \xi_i)^2 + y^2 + z^2 \right]^{3/2}} - \frac{Q_i (y - 2h)}{4\pi \left[(x - \xi_i)^2 + (y - 2h)^2 + z^2 \right]^{3/2}},$$
 (3)

where n is the number of sources and sinks located on the axis of symmetry and corresponding sources and sinks with opposite intensities, located above the water surface on the line (z = 0, y = 2h), see Fig. 1.

It follows from (1)-(3) that the vertical velocities on the undisturbed water surface (at z = 0) are equal to:

$$v_y(x, h, 0) = \frac{h}{2\pi} \sum_{i=1}^{n} \frac{Qz}{\left[(x - \xi_i)^2 + h^2\right]^{3/2}}.$$
 (4)

It was proposed in [8] to use formula (4) for estimations of the water surface deformations and wave resistance.

The pressure coefficient on the body surface at z=0 can be calculated as follows, [8]:

$$c_p(x, -R(x), 0) = \frac{2(p - p_{\infty})}{\rho U^2} = 1 - v_x^2(x, -R(x), 0) - v_y^2(x, -R(x), 0),$$
 (5)

where p and p_{∞} are the local pressure and the pressure at infinity at the same depth, ρ is the water density, R(x) is the body radius, $v_z(x, y, 0) = 0$. We will consider bodies of revolution

with convex and concave noses using the distributions of sources and sinks:

$$q_1(x) = \begin{cases} ax^2 + bx, & 0 \le x \le x_*; \\ a_1(x-1)^2, & x_* \le x \le 1, \end{cases}$$
 (6)

$$q_2(x) = \begin{cases} cx^3 + dx^4, & 0 \le x \le x_*; \\ a_1(x-1)^2, & x_* \le x \le 1, \end{cases}$$
 (7)

respectively. The values of constant parameters a, b, c, d, a_1 and x_* can be adjusted to obtain shapes with different L/D ratios. In particular, a shape similar to the sailfish trunk was calculated in [8] and corresponding vertical velocities on the water surface and pressure distributions on the body surface were found with the use of eqs. (4) and (5). In this study, we will consider shapes with smaller and larger values of L/D to confirm the findings of papers [8,22]. The absence of stagnation points on the concave noses of axisymmetric bodies with different L/D values was demonstrated in [7] for the unbounded flow. Here we will show that the same applies to bodies moving near the water surface.

3. CALCULATION OF PRESSURE DISTRIBUTION THE BODY SURFACE AT DIFFERENT DEPTH OF MOVEMENT

Figs. 2 and 3 illustrate the pressure distributions (5) on the surfaces of bodies of revolution with two different aspect ratios ($L/D \approx 5.3$ and $L/D \approx 27$, respectively). 'Circles' represent the pressure coefficient on shapes with convex noses (calculated with the use of distribution (6) and shown by dashed lines); 'triangles' correspond to shapes with concave noses (calculated with the use of distribution (7) and shown by solid lines). The size of the markers used in Figs. 2 and 3 increases with the dimensionless depth h/L; the largest ones represent the case of unbounded flow or infinite depth.

It can be seen that there are no stagnation points (and pressure peaks) on concave noses (compare 'triangles' and 'crosses' in Figs. 2 and 3) at all values of the depth. In comparison, $c_p \to 1.0$ near the stagnation points (not shown in the figures). The same result was obtained in [8] for the body of revolution similar to sailfish (L/D=10). The absence of high pressures allows us to expect a low wave resistance since pressure peaks create the waves on the water surface [23–25]. In the next section, we will calculate the vertical velocities on the water surface to estimate the amplitude of these waves.

Negative pressure gradients are visible on all shapes upstream and downstream of the maximum diameter section. This peculiarity probably prevents the separating of the boundary layer (as demonstrated experimentally for a dolphin-like shape, [6]). On the other hand, concave noses yield zones with positive pressure gradients in their vicinity (see 'triangles' in Figs. 2 and 3). A possible separation in these zones needs further investigation.

4. CALCULATION OF VERTICAL VELOCITIES ON THE WATER SURFACE AT DIFFERENT DEPTH OF MOVEMENT

Figs. 4 and 5 illustrate the results of calculations of the dimensionless vertical velocities (based on the speed of movement U) on the undisturbed water with the use of eq. (4) upstream of the axisymmetric bodies with two different aspect ratios ($L/D \approx 5.3$ and $L/D \approx$

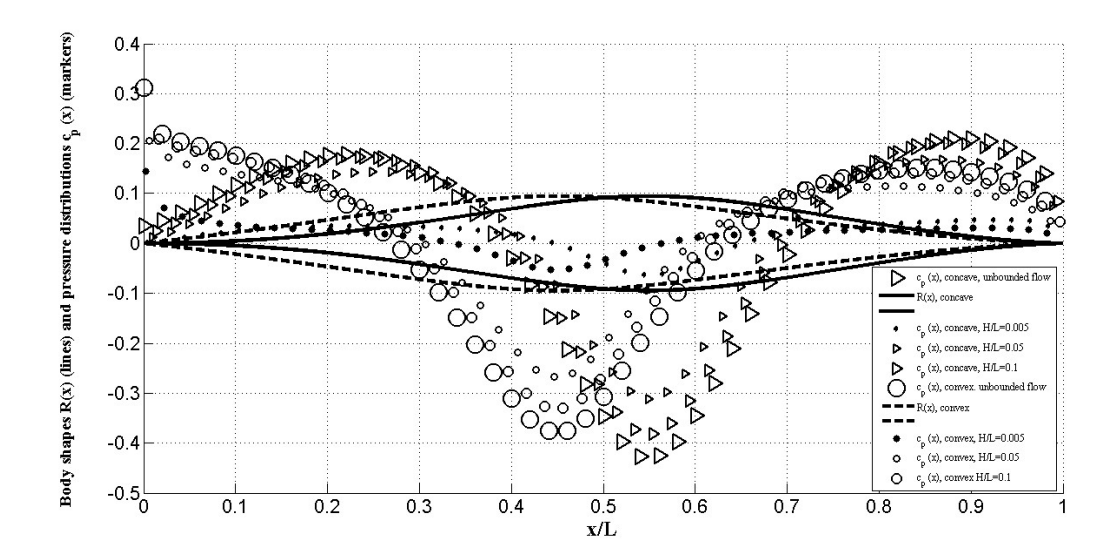


Fig. 2. Bodies with L/D = 5.3 and concave (solid lines and 'triangles') and convex (dashed lines and 'circles') noses. Lines represent the body radii R(x), markers represent the pressure coefficients on the body surfaces $.c_p(x, -R(x), 0)$ at different depths of movement h/L, Eq. (5). The size of markers increases with the increase of depth (the largest ones correspond to the infinite depth (unbounded flow))

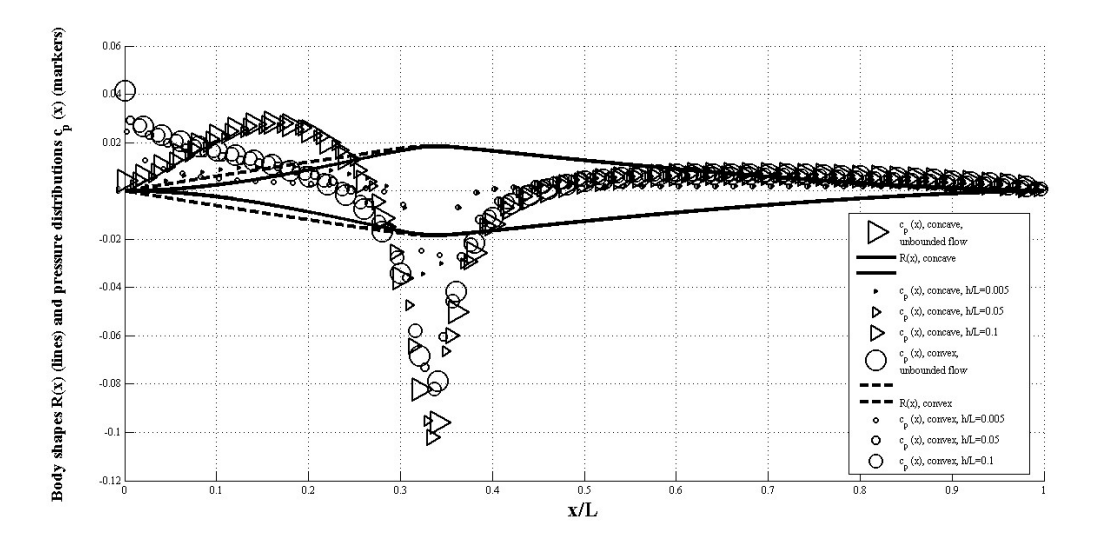


Fig. 3. Slender bodies with L/D=27 and concave (solid lines and 'triangles') and convex (dashed lines and 'circles') noses. Lines represent the body radii R(x), markers represent the pressure coefficients on the body surfaces $c_p(x, -R(x), 0)$ at different depths of movement h/L, Eq. (5). The size of markers increases with the increase of depth (the largest ones correspond to the infinite depth (unbounded flow))

27, respectively). 'Circles' represent the vertical velocities for shapes with convex noses (calculated with the use of distribution (6) and shown in Figs. 2 and 3 by dashed lines); 'triangles' correspond to shapes with concave noses (calculated with the use of distribution (7) and shown in Figs. 2 and 3 by solid lines). The size of markers increases with dimensionless depth h/L.

It can be seen that bodies with concave noses cause much lower values of the vertical velocities on the water surface in comparison with convex noses at the same values of the depth (compare 'triangles' and 'crosses' in Figs. 4 and 5). The same result was obtained in [8] for the body of revolution similar to sailfish (L/D=10). Since lower vertical velocities correspond to smaller deformations of the water surface, we can expect lower values of wave resistance on bodies with concave noses. As expected, more slender bodies (with lower magnitudes of the pressure of their surface) yield lower values of the vertical velocity (compare markers in Figs. 4 and 5).

Figs. 6 and 7 illustrate the results of calculations of the dimensionless vertical velocities (based on the speed of movement U) on the undisturbed water with the use of eq. (4) downstream of the axisymmetric bodies with two different aspect ratios ($L/D \approx 5.3$ and $L/D \approx 27$, respectively). 'Circles' represent the vertical velocities for shapes with the convex nose (calculated with the use of distribution (6) and shown in Figs. 2 and 3 by dashed lines); 'triangles' correspond to shapes with the concave nose (calculated with the use of distribution (7) and shown in Figs. 2 and 3 by solid lines). The size of markers increases with the increase of the dimensionless depth h/L.

The magnitudes of vertical velocities downstream of the body with a concave nose and $L/D \approx 5.3$ (shown in Fig. 2 by the solid line) can be higher than upstream at the same depth (compare 'triangles' in Figs. 4 and 6). It is a result of higher pressure near the tail (visible in Fig. 2). The corresponding values of $|v_y(x, h, 0)|$ are higher than for the body with a convex nose (shown in Fig. 2 by the dashed line) at the same values of the depth (compare 'crosses' and 'triangles' in Fig. 6) due to the higher c_p values near the tail lower (compare 'crosses' and 'triangles' in Fig. 2).

The magnitudes of vertical velocities downstream of both slender bodies with $L/D \approx 27$ are very close (compare 'crosses' and 'triangles' in Fig. 7) and are much lower than upstream (compare markers in Figs. 5 and 7) due to the similar and low c_p values near their tails (visible in Fig. 3). The same result was obtained in [8] for a body of revolution similar in shape to that of sailfish (L/D = 10).

5. ESTIMATION OF THE TOTAL DRAG ON SPECIAL SHAPED FLOATING BODIES OF REVOLUTION WITH CONCAVE NOSES

Since high pressures on the ship hull cause the water surface deformations and wave resistance [23–25], very slender wave-piercing hulls and bulbous bows are used [26–28]. At the same time, it is of interest to improve the shape of the hulls with constant elongation (L/D ratio) and without using bulbous bows (to minimize added resistance in waves). The proposed shapes with very thin concave noses yield the solution and open the perspectives for significantly reducing wave resistance. In particular, it is possible to recommend underwater hull shapes similar to that shown by solid lines in Figs. 2 and 3 with a waterline providing small values of depth h. Then we can expect very small values of wave resistance since

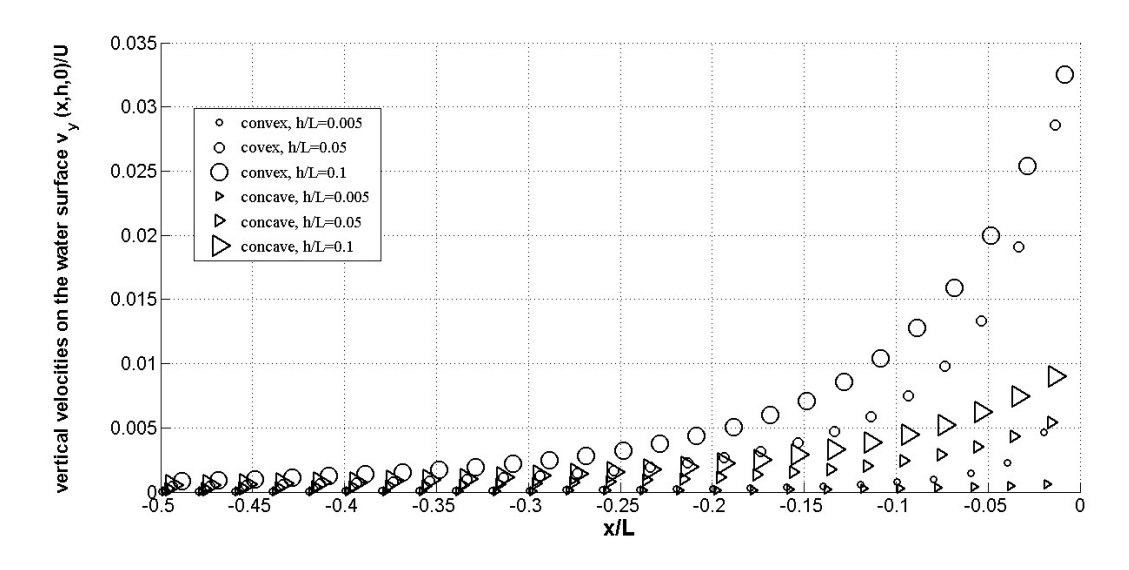


Fig. 4. Vertical velocities on the water surface upstream of the bodies with L/D=5.3 and concave ('triangles') and convex ('circles') noses at different depths of movement h/L, Eq. (4). The size of markers increases with the depth

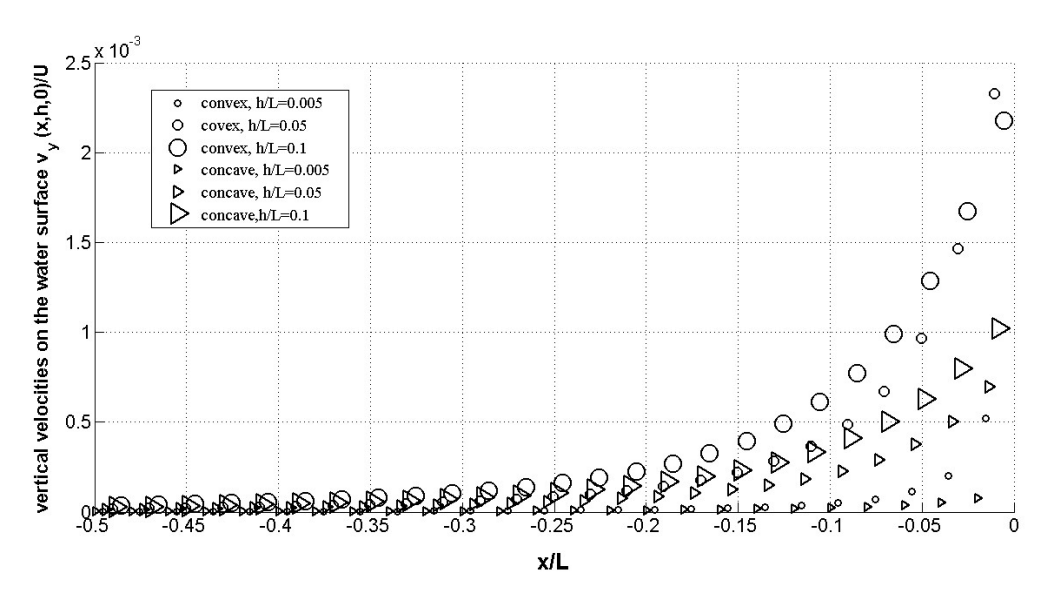


Fig. 5. Vertical velocities on the water surface upstream of the slender bodies with L/D = 27 and concave ('triangles') and convex ('circles') noses at different depths of movement h/L, Eq. (4). The size of markers increases with the depth

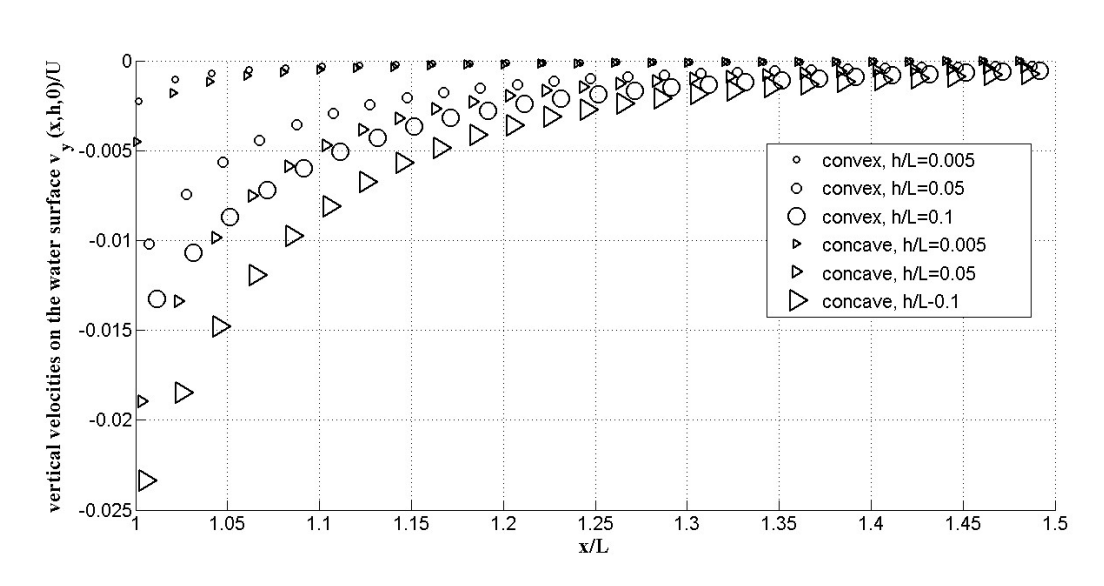


Fig. 6. Vertical velocities on the water surface downstream of the bodies with L/D = 5.3 and concave ('triangles') and convex ('circles') noses at different depths of movement h/L, Eq. (4). The size of markers increases with the depth

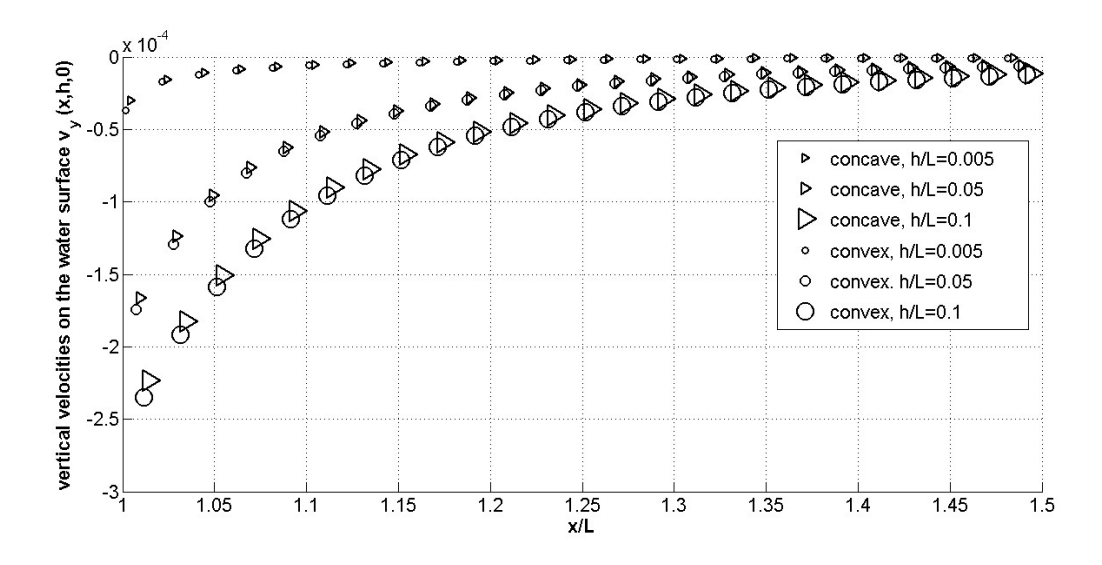


Fig. 7. Vertical velocities on the water surface downstream of the slender bodies with L/D = 27 and concave ('triangles') and convex ('circles') noses at different depths of movement h/L, Eq. (4). The size of markers increases with the depth

the absolute values of vertical velocities on the water surface and its deformation will be minimal.

The nature of the flow around such hulls requires further experimental research, but the similarity of their shape to the shape of the body of high-speed fish [2, 19–21] allows us to have a laminar flow without separation of the boundary layer and minimal total resistance. Let us evaluate this drag and the economic efficiency of vessels with laminar hulls. We will also estimate the maximum speed of such vehicles.

Let us use the formula for the total drag X on the slender body of revolution with volume V in the laminar unbounded flow of incompressible fluid with velocity at infinity U. Since pressure drag can be neglected in the flows without boundary-layer separation and the wave drag at large values of depth tends to zero, the total drag is close to friction one. In particular, the volumetric characteristics can be written as follows [1]:

$$C_V = \frac{2X}{\rho U^2 V^{2/3}} = \frac{4.7}{\sqrt{\text{Re}_V}}, \qquad \text{Re}_V = \frac{UV^{1/3}}{\nu}.$$
 (8)

Here ν is the kinematic viscosity of water. Formula (8) is valid only for values of the volumetric Reynolds numbers Re_V , which are lower than the critical one, [1]:

$$Re_V^* = \frac{59558\pi L^2}{V^{2/3}}. (9)$$

At a small value of depth h, approximately half of an axisymmetric body is wetted by water. Then we can assume that the drag of the corresponding floating hull is approximately twice lower, and its displacement W is approximately half of the volume V, i.e.:

$$W \approx 0.5V. \tag{10}$$

According to formula (8) the volumetric drag coefficient of the floating hull is $2^{1/3}$ lower, i.e., taking into account (10), the following equations can be used:

$$C_W \approx \frac{C_V}{2^{1/3}} = \frac{4.7}{2^{1/3}\sqrt{\text{Re}_V}} = \frac{4.7}{\sqrt{2\text{Re}_W}} = \frac{3.3}{\sqrt{\text{Re}_W}}, \quad \text{Re}_W = \frac{UW^{1/3}}{\nu}.$$
 (11)

The first formula in Eq. (11) shows that for special unseparated laminar hulls, their volumetric drag coefficient is independent of their shapes (in particular, independent of the aspect ratio L/D) and can be very small at high Reynolds numbers.

To check this very important point, let us use the flat plate concept [29], which supposes that friction drag X_f on the axisymmetric body can be estimated using the drag coefficient on the flat plate and the area S wetted by water. Using the Blasius solution [9] for the laminar friction drag coefficient, the corresponding drag coefficient C_{xS} (based on the area S of the body of revolution wetted by water) can be written as follows:

$$C_{xS} = \frac{2X_f}{\rho U^2 S} \approx \frac{1.328}{\sqrt{\text{Re}_L}}, \qquad \text{Re}_L = \frac{UL}{\nu}.$$
 (12)

Using the volumetric characteristics (based on the displacement W) and neglecting the wave resistance, for the total drag X formulae (12) can be rewritten as follows:

$$C_W = \frac{2X}{\rho U^2 W^{2/3}} \approx \frac{k_s}{\sqrt{\text{Re}_W}}, \qquad k_s = \frac{1.328S}{\sqrt{WL}}.$$
 (13)

In comparison to the first formula (11), the flat plate concept yields some dependence on the shape due to the coefficient k_s . The values of the shape coefficient k_s vary from 2.65 to 2.85 for bodies of revolution shown in Figs. 2 and 3. Thus, the flat plate concept yields lower values of the drag in comparison with formula (11) ($k_s = 3.3$). Applying this concept to the slender elliptical bodies of revolution and using empirical Hoerner equations, [29]:

$$W = 0.65\pi LD^2/8, \qquad S \approx 0.75L\pi D/2$$
 (14)

we can obtain $k_s = 3.1$.

Thus, Eq. (11) can be used to estimate the total drag on specially shaped bodies of revolution with concave noses floating at small values of depth. The minimal values of the volumetric drag coefficient correspond to the maximum of Re_W . Since the estimate in Eq. (11) is valid only for laminar flow, the minimum of C_W corresponds to the critical Reynolds number and with the use of Eqs. (9)–(11) can be estimated as follows:

$$C_W^{(\min)} \approx 0.011 \frac{W^{1/3}}{L}.$$
 (15)

Eq. (15) shows that the lowest drag coefficients correspond to the very slender bodies (with high aspect ratio L/D and small W/L^3 values). For example, for specially shaped bodies with concave noses ($L/D \approx 5.3$ and $L/D \approx 27$, see solid lines in Figs. 2 and 3) formula (15) yields $C_W^{(\text{min})}$ equal to 0.0023 and 0.00073, respectively. Unfortunately, a drag coefficient of such low magnitude can only be achieved for rather small ships. With the use of Eqs. (9) and (10) we can estimate the critical (maximal) displacement of the laminar hull of length L moving at speed U and small values of depth:

$$W^* = \frac{29779\pi\nu L^2}{U}. (16)$$

If we fix the speed at 15 m/s and L=10 m, then at $\nu=1.3\cdot 10^{-6}$ m²/s, Eq. (16) yields $W^*=0.81$ m³. According to Eq. (15), the volumetric drag coefficient of such a boat can be estimated as 0.0009. For longer ships (e.g., L=100 m), the maximal displacement of a laminar hull is 81 m³ and $C_W^{(\text{min})}=0.00042$ (at the same speed 15 m/s). Even for superlong ships (e.g., L=500 m), the displacement of a laminar hull is only 2025 m³ and $C_W^{(\text{min})}=0.00024$. The aspect ratios of the longer and super longer laminar hulls must be much higher than for the slender body shown in Fig. 3. It could be difficult to manufacture such very elongated hulls and ensure their strength and stability. At smaller speeds (e.g., U=10 m/s), the corresponding displacements are 1.5 times higher.

Using multiple slender hulls (see, e.g. [30]) allows increasing the displacement. Nevertheless, the drag coefficient of such ships also increases. For example, the use of n equal hulls each of displacement W increases the drag n times, and the corresponding volumetric drag coefficient $C_W^{(n)}$

$$C_W^{(n)} = \frac{2nX}{\rho U^2 (nW)^{2/3}} = n^{1/3} C_W \tag{17}$$

 $n^{1/3}$ times (the interference of hulls is neglected).

6. SPEED LIMITATIONS FOR EFFECTIVE FLOATING VEHICLES WITH SPECIALLY SHAPED HULLS

The expected low values of the wave resistance on special-shaped hulls with concave noses allow us to go beyond the well-known limit for the Froude number $\operatorname{Fr}_L^* = U/\sqrt{gL} \approx 0.4$. Its exceeding causes the drastic increase of the wave resistance on standard hulls with stagnation points, [31]. On the other hand, there are some limitations connected with the economical efficiency: the drag-to-weight ratio 1/k [1,32]. The vehicle with the minimal value of this ratio ensures the maximum of ton-kilometers per unit of time [32]. At a fixed amount of fuel (or electrical energy) on board, a vehicle with a maximum value of k has the maximum range [1].

Replacing V by W in corresponding formulas of paper [1] and taking into account Eq. (10), we can obtain

$$\frac{1}{k} = \frac{1 - \alpha}{k_W} + \frac{C_W \rho U^2 W^{2/3}}{2mg} = \frac{1 - \alpha}{k_W} + 0.5\alpha C_W \operatorname{Fr}_W^2, \quad \alpha = \frac{\rho W}{m}, \quad \operatorname{Fr}_W^2 = \frac{U^2}{gW^{1/3}} = \frac{\operatorname{Fr}_L^2 L}{W^{1/3}}, \quad (18)$$

where k_W is the ratio of the lifting force to the drag. For a neutral buoyant vehicle $\alpha = 1$. Then for a ship with the special shaped laminar hull, Eqs. (11) and (18) yield:

$$k \approx \frac{0.6\sqrt{\text{Re}_W}}{Fr_W^2} = \frac{0.6gW^{1/2}}{U^{3/2}\nu^{1/2}}.$$
 (19)

Formula (19) shows that the increase of commercial efficiency can be achieved by decreasing speed and increasing displacement. For example, at $W = 1 \text{ m}^3$ and $\nu = 1.3 \cdot 10^{-6} \text{ m}^2/\text{s}$ we can obtain k = 163 at speed 10 m/s and k = 31 at U = 30 m/s. Thus, the ships with new hulls will be rather effective even at high values of the velocity, since for planning vehicles it is practically impossible to achieve values of the lift-to-drag ratio k_W greater than 20.

Since the commercial efficiency increases at higher Reynolds numbers (see Eq. (19)), which are limited by Eq. (9), then its maximal value k_{max} corresponds to the critical Reynolds number. Using Eqs. (9) and (19) yields:

$$k_{\text{max}} \approx 206 \text{Fr}_L^{-2}. \tag{20}$$

Formula (20) shows that the maximal value of the commercial efficiency depends only on the Froude number. In particular, the shape and the use of multiple laminar hulls with the concave nose do not change the value of $k_{\text{max}} = k_{\text{max}}^{(n)}$.

At large Froude numbers the commercial efficiency of neutral buoyant vehicles decreases. Then the planning vehicles can become more effective. Taking the maximum value $k_W = 20$ for planning boats we can calculate the maximal Froude number for effective neutral buoyant ships with special shaped hulls:

$$\operatorname{Fr}_{L,\max} \approx 3.2.$$
 (21)

For example, according to (21) at speed 20 m/s the length of effective boats must be grater than 4 m.

The speed of any vehicle is limited by the power of its engine. The ratio p_W of the engine power to its weight (including the weight of fuel or electrical batteries) is the most

important characteristic to estimate the maximal speed. Taking into account that only a part $0 < k_P \le 1$ of engine power $0 < k_P \le 1$ can be transformed to the power of steady motion XU of a vehicle and the fact that the weight of the engine together with the weight of the fuel (or accumulators) gm_a is only a part $0 < k_m \le 1$ of the total vehicle weight, the following relationships can be written, [22]:

$$p_W = \frac{P_a}{gm_a} = \frac{XU}{k_P k_m mg} = \frac{XU}{k_P k_m \rho Wg} = \frac{\rho C_W U^2 W^{2/3} U}{2k_P k_m \rho Wg} = \frac{C_W U^3}{2k_P k_m g W^{1/3}}.$$
 (22)

Eq. (22) allows estimating the velocity, which can be achieved at given values of p_W , k_m , and k_P :

$$U = \sqrt[3]{\frac{2p_W k_P k_m g W^{1/3}}{C_W}} = \frac{k_t W^{1/9}}{C_W^{1/3}}, \qquad k_t = \sqrt[3]{2p_W k_P k_m g}.$$
 (23)

Formula (23) shows that the achievable velocity increases slowly with the increase of displacement and with diminishing the volumetric drag coefficient. For ships using new specially shaped laminar hulls with concave noses, we can substitute formula (11) for C_W into (23) to obtain:

$$U = 0.62 \frac{k_t^{6/5} W^{1/5}}{\nu^{1/5}}. (24)$$

Thus, the maximum velocity of such boats does not depend on the hull shape (in particular, shapes with different L/D values can be used) and very slightly increases with increasing their displacement.

Let us estimate the maximum possible speed of boats with the new hull shape, taking the value $p_W = 50$ m/s typical for turbocharged diesel engines [33], small outboard motors [34] and electrical accumulators [35]. If values k_P and k_m range between 0.1 and 1.0, then according to the second formula (23), k_t values will be between 2.1 and 9.9 m^{2/3}/s. Taking in (24) the minimal value $k_t = 2.1 \text{ m}^{2/3}/\text{s}$, $\nu = 1.3 \cdot 10^{-6} \text{ m}^2/\text{s}$ and $W = 0.3 \text{ m}^3$, the maximal speed of a specially shaped boat can be estimated as 17.9 m/s. The maximal velocity of a typical small dinghy is around 8 knots or 4.1 m/s [34].

At higher values of k_t and /or for larger specially shaped ships, higher speeds can be achieved (see, Eq. (24). This makes the problem of cavitation on the hull or propellers relevant. The critical speed of the cavitation inception U^* on the hull can be estimated with the use of condition $\sigma = -C_P^{(\min)}$ [36], where $C_P^{(\min)}$ is the minimum value of the pressure coefficient on the vehicle surface; $\sigma = 2p_{at}/(\rho U^2)$ is the cavitation number; the depth of movement and the pressure inside the cavity in comparison with the atmospheric pressure pat are neglected. On slender bodies shown in Fig. 3 $C_P^{(\min)} \approx -0.1$, then $U^* \approx 45$ m/s. Cavitation on propellers may start at lower velocities of ship movement. In particular, in the wake after the fastest passenger ship Francisco High-Speed Ferry [37] (U = 26.7 m/s; L = 99 m; Fr_L = 0.86), a huge amount of bubbles occurs. This phenomenon decreases commercial efficiency.

7. CONCLUSIONS

The pressure distributions on the specially shaped bodies of revolutions moving along the axis of symmetry near the water surface are calculated using the potentials of sources and

sinks. The absence of the stagnation points and a pressure increase on the sharp concave noses, similar in shape to the rostrums of the fastest fish, was illustrated. This allows for diminishing the vertical velocities on the water surface and wave resistance.

The calculated new shapes can be recommended for underwater parts of the ship hulls to reduce the total drag and improve commercial efficiency. The lowest values of drag and the highest efficiency correspond to the laminar flow pattern, for which estimations of the drag, commercial efficiency, displacement, and maximal speed are presented.

To check the obtained theoretical results, further experimental studies are necessary. In the case of success, the new special-shaped hull can be recommended for shipbuilding, in particular, to increase the speed and range of unmanned vehicles.

ACKNOWLEDGEMENTS

The author is grateful to Peter Thomas, Ulrike Tillmann, James Robinson, Robin Thompson, Matt Keeling, and Oleksii Rodionov for their support and providing very useful information. This paper was written with the support of the INI-LMS Solidarity Programme at the University of Warwick, UK.

REFERENCES

- [1] I. Nesteruk, "Efficiency of steady motion and its improvement with the use of unseparated and supercavitating flow patterns," Research Bulletin of the National Technical University of Ukraine "Kyiv Polytechnic Institute", no. 6, pp. 51–67, 2016. DOI: https://doi.org/10.20535/1810-0546.2016.6.81605
- [2] Y. G. Aleyev, *Nekton*. The Hague: Dr. W. Junk, 1977. DOI: https://doi.org/10.1007/978-94-010-1324-6
- [3] J. Rohr, M. I. Latz, S. Fallon, and J. C. Nauen, "Experimental approaches towards interpreting dolphin-stimulated bioluminescence," *Journal of Experimental Biology*, vol. 201, no. 9, pp. 1447–1460, 1998. DOI: https://doi.org/10.1242/jeb.201.9.1447
- [4] I. G. Nesteruk, "Rigid bodies without boundary-layer separation," International Journal of Fluid Mechanics Research, vol. 41, no. 3, pp. 260–281, 2014. DOI: https://doi.org/10.1615/interjfluidmechres.v41.i3.50
- [5] I. Nesteruk, "Maximal speed of underwater locomotion," *Innovative Biosystems and Bioengineering*, vol. 3, no. 3, pp. 152–167, 2019. DOI: https://doi.org/10.20535/ibb.2019.3.3.177976
- [6] I. G. Nesteruk, M. Brühl, and T. Moeller, "Testing a special shaped body of revolution similar to dolphins trunk," Research Bulletin of the National Technical University of Ukraine "Kyiv Politechnic Institute", no. 2, pp. 44–53, 2018. DOI: https://doi.org/10.20535/1810-0546.2018.2.129140
- [7] I. Nesteruk, "Fastest fish shapes and optimal supercavitating and hypersonic bodies of revolution," *Innovative Biosystems and Bioengineering*, vol. 4, no. 4, pp. 169–178, 2020. DOI: https://doi.org/10.20535/ibb.2020.4.4.215578

- [8] I. Nesteruk, "Shapes of the fastest fish and optimal underwater and floating hulls," Theoretical and Applied Mechanics Letters, vol. 12, no. 6, p. 100378, 2022. DOI: https://doi.org/10.1016/j.taml.2022.100378
- [9] L. G. Loitsyanskiy, Mechanics of liquids and gases. New York: Begell House, 1995. DOI: https://doi.org/10.1615/978-1-56700-042-9.0
- [10] L. D. Landau and E. M. Lifshitz, *Fluid mechanics*. Oxford, UK: Butterworth-Heinemann, 1987.
- [11] M. F. Zedan, A. A. Seif, and S. Al-Moufadi, "Drag reduction of fuselages through shaping by the inverse method," *Journal of Aircraft*, vol. 31, no. 2, pp. 279–287, 1994. DOI: https://doi.org/10.2514/3.46485
- [12] T. Lutz and S. Wagner, "Drag reduction and shape optimization of airship bodies," *Journal of Aircraft*, vol. 35, no. 3, pp. 345–351, 1998. DOI: https://doi.org/10.2514/2.2313
- [13] F. R. Goldschmied, "Integrated hull design, boundary-layer control and propulsion of submerged bodies: wind-tunnel verification," in *Proceedings of the AIAA/SAE/ASME 18th Joint Propulsion Conference*. AIAA, 1982, pp. 3–18. DOI: https://doi.org/10.2514/6.1982-1204
- [14] J. Gray, "Studies in animal locomotion VI. the propulsive powers of the dolphin," Journal of Experimental Biology, vol. 13, no. 2, pp. 192–199, 1936. DOI: https://doi.org/10.1242/jeb.13.2.192
- [15] F. E. Fish and J. J. Rohr, Review of dolphin hydrodynamics and swimming performance. TR 1801. San Diego, CA: SPAWARS, 1999. DOI: https://doi.org/10.21236/ada369158
- [16] F. E. Fish, "The myth and reality of Gray's paradox: implication of dolphin drag reduction for technology," *Bioinspiration & Biomimetics*, vol. 1, no. 2, pp. R17–R25, 2006. DOI: https://doi.org/10.1088/1748-3182/1/2/r01
- [17] F. E. Fish, P. Legac, T. M. Williams, and T. Wei, "Measurement of hydrodynamic force generation by swimming dolphins using bubble DPIV," *Journal of Experimental Biology*, vol. 217, no. 2, pp. 252–260, 2014. DOI: https://doi.org/10.1242/jeb.087924
- [18] R. Bale, M. Hao, A. P. S. Bhalla, N. Patel, and N. A. Patankar, "Gray's paradox: A fluid mechanical perspective," *Scientific Reports*, vol. 4, no. 1, p. 5904, 2014. DOI: https://doi.org/10.1038/srep05904
- [19] R. K. Logan, S. M. Luongo, J. J. Vaudo, B. M. Wetherbee, and M. S. Shivji, "Hunting behavior of a solitary sailfish Istiophorus platypterus and estimated energy gain after prey capture," *Scientific Reports*, vol. 13, no. 1, p. 1484, 2023. DOI: https://doi.org/10.1038/s41598-023-28748-0

- [20] S. R. Tracey, B. W. Wolfe, K. Hartmann, J. Pepperell, and S. M. Williams, "Movement behavior of swordfish provisions connectivity between the temperate and tropical southwest Pacific Ocean," *Scientific Reports*, vol. 13, no. 1, p. 11812, 2023. DOI: https://doi.org/10.1038/s41598-023-38744-z
- [21] C. A. Rohner, R. Bealey, B. M. Fulanda, J. D. Everett, A. J. Richardson, and S. J. Pierce, "Movement ecology of black marlin Istiompax indica in the Western Indian Ocean," *Journal of Fish Biology*, vol. 99, no. 3, pp. 1044–1059, 2021. DOI: https://doi.org/10.1111/jfb.14809
- [22] I. Nesteruk, S. Krile, and T. Möller, "Improved low-drag pontoons for water bikes," Journal of Marine Science and Engineering, vol. 11, no. 9, p. 1754, 2023. DOI: https://doi.org/10.3390/jmse11091754
- [23] L. Larsson, H. C. Raven, and J. R. Paulling, Eds., *Ship resistance and flow*, ser. Principles of naval architecture. Jersey City, NJ: SNAME, 2010.
- [24] T. H. Havelock, "Wave patterns and wave resistance," Transactions of the Royal Institution of Naval Architects, pp. 430–442, 1934.
- [25] E. O. Tuck, J. L. Collins, and W. H. Wells, "On ship waves and their spectra," Journal of Ship Research, vol. 15, pp. 11–21, 1971. DOI: https://doi.org/10.5957/jsr.1971.15.1.11
- [26] E. Boulougouris and A. Papanikolaou, "Hull form optimization of a high-speed wave piercing monohull," in *Proceedings of the 9th International Marine Design Conference IMDC06*, Ann Arbor, MI, 2006, pp. 1–21.
- [27] C. Wei, Y. Li, S. Yu, and H. Yi, "Experimental study on the high speed mono-wave-piercing boat," *Journal of Shanghai Jiaotong University (Science)*, vol. 21, no. 5, pp. 524–529, 2016. DOI: https://doi.org/10.1007/s12204-016-1758-4
- [28] A. Grech La Rosa, "Reinventing the bulbous bow," phdthesis, University College London, London, 2023.
- [29] S. F. Hoerner, Fluid-dynamic drag. Midland Park, NJ: Published by the Author, 1965.
- [30] L. Lazauskas and E. O. Tuck, "Low drag multihulls for sporting, commercial and military applications," in *Proceedings of the Fourth International Conference on Fast Sea Transport (FAST97)*. Melbourne: Baird Publications, 1997, pp. 647–652.
- [31] Q. Zeng, R. Hekkenberg, C. Thill, and H. Hopman, "Scale effects on the wave-making resistance of ships sailing in shallow water," *Ocean Engineering*, vol. 212, p. 107654, 2020. DOI: https://doi.org/10.1016/j.oceaneng.2020.107654
- [32] Y. Gabrielly and T. von Karman, "What price speed? specific power required for propulsion of vehicles," *Mechanical Engineering*, *USA*, vol. 72, no. 10, pp. 775–779, 1950.

- [33] Internet Archive. Engine specifications. [Online]. Available: https://web.archive.org/web/20121102194334/http://eogld.ecomm.gm.com/images/mediumduty/techspecs/engine.pdf
- [34] BoatUS. The evolution of outboard engines: look at and future developments. [Online]. Available: past, present, https://www.boatus.com/expert-advice/expert-advice-archive/2023/april/theevolution-of-outboard-engines
- [35] J. Ajuria, E. Redondo, M. Arnaiz, R. Mysyk, T. Rojo, and E. Goikolea, "Lithium and sodium ion capacitors with high energy and power densities based on carbons from recycled olive pits," *Journal of Power Sources*, vol. 359, pp. 17–26, 2017. DOI: https://doi.org/10.1016/j.jpowsour.2017.04.107
- [36] R. T. Knapp, J. W. Daily, and F. G. Hammitt, Cavitation. New York: McGraw Hill, 1970.
- [37] Ship Technology. (2021) Francisco Papa high-speed ferry. [Online]. Available: https://www.ship-technology.com/projects/francisco-high-speed-ferry/

ЛІТЕРАТУРА

- [1] Nesteruk I. Efficiency of steady motion and its improvement with the use of unseparated and supercavitating flow patterns // Наукові вісті НТУУ КПІ. 2016. № 6. С. 51—67.
- [2] Aleyev Y. G. Nekton. The Hague : Dr. W. Junk, 1977. 435 p.
- [3] Experimental approaches towards interpreting dolphin-stimulated bioluminescence / Rohr J., Latz M. I., Fallon S., and Nauen J. C. // Journal of Experimental Biology.— 1998.—Vol. 201, no. 9.—P. 1447–1460.
- [4] Nesteruk I. G. Rigid bodies without boundary-layer separation // International Journal of Fluid Mechanics Research. 2014. Vol. 41, no. 3. P. 260–281.
- [5] Nesteruk I. Maximal speed of underwater locomotion // Innovative Biosystems and Bioengineering. 2019. Vol. 3, no. 3. P. 152–167.
- [6] Nesteruk I. G., Brühl M., Moeller T. Testing a special shaped body of revolution similar to dolphins trunk // Haykobi Bicti HTYY KIII. $-2018. N \cdot 2. C. 44-53.$
- [7] Nesteruk I. Fastest fish shapes and optimal supercavitating and hypersonic bodies of revolution // Innovative Biosystems and Bioengineering. 2020. Vol. 4, no. 4. P. 169–178.
- [8] Nesteruk I. Shapes of the fastest fish and optimal underwater and floating hulls // Theoretical and Applied Mechanics Letters. 2022. Vol. 12, no. 6. P. 100378.
- [9] Лойцянский Л. Г. Механика жидкости и газа. Москва : Наука, 1987. 840 с.

- [10] Ландау Л. Д., Лифшиц Е. М. Гидродинамика. Москва : Наука, 1986. 736 с.
- [11] Zedan M. F., Seif A. A., Al-Moufadi S. Drag reduction of fuselages through shaping by the inverse method // Journal of Aircraft. 1994. Vol. 31, no. 2. P. 279–287.
- [12] Lutz T., Wagner S. Drag reduction and shape optimization of airship bodies // Journal of Aircraft. 1998. Vol. 35, no. 3. P. 345–351.
- [13] Goldschmied F. R. Integrated hull design, boundary-layer control and propulsion of submerged bodies: wind-tunnel verification // Proceedings of the AIAA/SAE/ASME 18th Joint Propulsion Conference. AIAA. 1982. P. 3–18.
- [14] Gray J. Studies in animal locomotion VI. The propulsive powers of the dolphin // Journal of Experimental Biology. 1936. Vol. 13, no. 2. P. 192–199.
- [15] Fish F. E., Rohr J. J. Review of dolphin hydrodynamics and swimming performance. TR 1801.—San Diego, CA: SPAWARS, 1999.
- [16] Fish F. E. The myth and reality of Gray's paradox: implication of dolphin drag reduction for technology // Bioinspiration & Biomimetics. 2006. Vol. 1, no. 2. P. R17–R25.
- [17] Measurement of hydrodynamic force generation by swimming dolphins using bubble DPIV / Fish F. E., Legac P., Williams T. M., and Wei T. // Journal of Experimental Biology. 2014. Vol. 217, no. 2. P. 252–260.
- [18] Gray's paradox: A fluid mechanical perspective / Bale R., Hao M., Bhalla A. P. S., Patel N., and Patankar N. A. // Scientific Reports. 2014. Vol. 4, no. 1. P. 5904.
- [19] Hunting behavior of a solitary sailfish Istiophorus platypterus and estimated energy gain after prey capture / Logan R. K., Luongo S. M., Vaudo J. J., Wetherbee B. M., and Shivji M. S. // Scientific Reports. 2023. Vol. 13, no. 1. P. 1484.
- [20] Movement behavior of swordfish provisions connectivity between the temperate and tropical southwest Pacific Ocean / Tracey S. R., Wolfe B. W., Hartmann K., Pepperell J., and Williams S. M. // Scientific Reports. 2023. Vol. 13, no. 1. P. 11812.
- [21] Movement ecology of black marlin Istiompax indica in the Western Indian Ocean / Rohner C. A., Bealey R., Fulanda B. M., Everett J. D., Richardson A. J., and Pierce S. J. // Journal of Fish Biology. 2021. Vol. 99, no. 3. P. 1044–1059.
- [22] Nesteruk I., Krile S., Möller T. Improved low-drag pontoons for water bikes // Journal of Marine Science and Engineering. 2023. Vol. 11, no. 9. P. 1754.
- [23] Ship resistance and flow / ed. by Larsson L., Raven H. C., Paulling J. R. Principles of naval architecture. Jersey City, NJ: SNAME, 2010. 230 p.
- [24] Havelock T. H. Wave patterns and wave resistance // Transactions of the Royal Institution of Naval Architects. 1934. P. 430–442.

- [25] Tuck E. O., Collins J. L., Wells W. H. On ship waves and their spectra // Journal of Ship Research. 1971. Vol. 15. P. 11–21.
- [26] Boulougouris E., Papanikolaou A. Hull form optimization of a high-speed wave piercing monohull // Proceedings of the 9th International Marine Design Conference IMDC06. Ann Arbor, MI. 2006. P. 1–21.
- [27] Experimental study on the high speed mono-wave-piercing boat / Wei C., Li Y., Yu S., and Yi H. // Journal of Shanghai Jiaotong University (Science). 2016. Vol. 21, no. 5. P. 524–529.
- [28] Grech La Rosa A. Reinventing the bulbous bow: Ph. D. thesis; University College London. London, 2023.
- [29] Hoerner S. F. Fluid-dynamic drag. Midland Park, NJ: Published by the Author, 1965. 465 p.
- [30] Lazauskas L., Tuck E. O. Low drag multihulls for sporting, commercial and military applications // Proceedings of the Fourth International Conference on Fast Sea Transport (FAST97). Melbourne: Baird Publications. 1997. P. 647–652.
- [31] Scale effects on the wave-making resistance of ships sailing in shallow water / Zeng Q., Hekkenberg R., Thill C., and Hopman H. // Ocean Engineering. 2020. Vol. 212. P. 107654.
- [32] Gabrielly Y., von Karman T. What price speed? Specific power required for propulsion of vehicles // Mechanical Engineering, USA.—1950.—Vol. 72, no. 10.—P. 775–779.
- [33] Internet Archive. Engine specifications. [Онлайн]. Режим доступу: https://web.archive.org/web/20121102194334/http://eogld.ecomm.gm.com/images/mediumduty/techspecs/engine.pdf
- [34] BoatUS. The evolution of outboard look engines: at past, present. future developments. [Онлайн]. Режим доступу: https://www.boatus.com/expert-advice/expert-advice-archive/2023/april/theevolution-of-outboard-engines
- [35] Lithium and sodium ion capacitors with high energy and power densities based on carbons from recycled olive pits / Ajuria J., Redondo E., Arnaiz M., Mysyk R., Rojo T., and Goikolea E. // Journal of Power Sources. 2017. Vol. 359. P. 17–26.
- [36] Knapp R. T., Daily J. W., Hammitt F. G. Cavitation. New York: McGraw Hill, 1970. 578 p.
- [37] Ship Technology. Francisco Papa high-speed ferry. 2021. [Онлайн]. Режим доступу: https://www.ship-technology.com/projects/francisco-high-speed-ferry/

І. Г. Нестерук

Спеціально спрофільовані ламінарні корпуси малого опору для збільшення швидкості та комерційної ефективності плаваючих апаратів

Тонкі тіла обертання з приєднаним примежовим шаром можуть затримувати його турбулізацію й забезпечують низький опір тиску. Тому дослідження безвідривних твердих тіл, подібних до обводів водних тварин, дозволило зробити висновок, що сама форма може забезпечувати низький опір, властивий ламінарній течії. Об'ємний коефіцієнт опору тертя видовжених осесиметричних безвідривних корпусів досягає свого мінімуму при критичному числі Рейнольдса, яке пов'язує їхню швидкість, об'єм і довжину з кінематичною в'язкістю рідини та може використовуватися для оптимізації в необмежених потоках води або повітря. Характеристики запропонованих корпусів, що рухаються по поверхні води, поки невідомі. Тим не менш, було показано, що спеціальні форми з дуже гострими увігнутими носиками, схожі на роструми найшвидших риб, дозволяють усунути точки гальмування й високий тиск на поверхні тіла. Цей ефект дозволяє зменшити хвильовий опір. Потенціальний безвідривний потік нев'язкої нестисливої рідини навколо тонкого тіла обертання, що рухається горизонтально з постійною швидкістю поблизу поверхні води, моделювався з використанням джерел і стоків, розташованих на осі симетрії, та джерел і стоків протилежної інтенсивності, розташованих на відповідній лінії вище поверхні води. Продемонстровано відсутність піків тиску та малі значення вертикальної складової швидкості на водній поверхні для тіл обертання особливої форми з гострими увігнутими носиками для різних значень видовження та глибини руху. Для порівняння, ті ж характеристики були розраховані для форм з опуклими носиками. Оцінено повний опір, комерційну ефективність і максимальну водотоннажність ламінарного корпуса. Низькі значення повного опору дозволяють отримати досить високі швидкості руху при використанні стандартних двигунів. Після відповідних випробувань запропоновані форми можуть використовуватись для зменшення повного опору суден і веслувальних човнів, а також для підвищення швидкості та комерційної ефективності.

КЛЮЧОВІ СЛОВА: комерційна ефективність, зменшення опору, захист навколишнього середовища, нероздільні форми, хвильовий опір